Journal of Materials Chemistry A

RSC Publishing

PAPER

Flexible and transparent free-standing films with enhanced magnetic and luminescent anisotropy†

Cite this: *J. Mater. Chem. A*, 2013, **1**, 4786

Yibo Dou, Xiaoxi Liu, Mingfei Shao, Jingbin Han* and Min Wei

Flexible and robust free-standing films are fabricated *via* layer-by-layer (LBL) assembly of layered double hydroxide (LDH) nanoplatelets, poly(vinyl alcohol) (PVA) and a styrylbiphenyl derivative (BTBS), and show enhanced magnetic and luminescent anisotropy simultaneously. UV-vis absorption and fluorescence spectra demonstrate a stepwise and regular growth of the films upon increasing the number of deposition cycles. XRD, AFM and SEM indicate that the films possess a periodic layered and uniform surface morphology. In contrast to the disordered LDH/PVA/BTBS film prepared by a solvent evaporation method, the $(LDH/PVA/LDH/BTBS)_n$ films with ordered structures exhibit enhanced magnetic and optical properties, including higher saturation magnetization, longer luminescence lifetime and stronger polarized photoemission. Moreover, owing to the highly arrayed 2D-organized structure formed through LBL assembly, the presence of the free-standing film means that the alignment of the spins of the LDH nanoplatelets in random directions is avoided and imparts a high level of dispersion and orientation to the BTBS, which displays enhanced magnetic and luminescent anisotropy. Therefore, this work provides a facile method for the fabrication of anisotropic 2D-organized materials based on the LDH/PVA/LDH/BTBS system, which can be potentially used in magneto-optical sensors, magnetic data storage and magneto-resistive devices.

Received 29th December 2012
Accepted 7th February 2013

DOI: 10.1039/c3ta01674a

www.rsc.org/MaterialsA

1 Introduction

Transparent magneto-optical materials have attracted tremendous attention due to their high potential for magnetic data storage, optical isolators, optical switches and magneto-resistive devices.[1–3] In order to achieve high-performance magneto-optical materials, an oriented nanostructure with anisotropic properties is generally required.[4,5] Thus, the ability to direct the orientation, conformation and interaction of nanoscale building blocks is the key element in this research.[6–8] However, traditional processing techniques usually lead to films with a random orientation of building blocks in a wide variety of conformations, creating essentially isotropic materials.[9–11] Although researchers have rationally designed composites with single magnetic or optical anisotropy, how to achieve film materials with magnetic and luminescent anisotropy simultaneously still remains a challenging goal.

During the past decade, 2D nanostructured materials have attracted intense research activity because of their unique structural anisotropic properties.[12–14] Layered double hydroxides (LDHs) are one important type of layered material, whose structure can be generally expressed as $[M^{II}_{1-x}M^{III}_{x}(OH)_2](A^{n-})_{x/n}\cdot mH_2O$ (M^{II} and M^{III} are divalent and trivalent metals, respectively, A^{n-} is an interlayered anion).[15–17] Recently, LDH-based functional materials have been widely used in biological, optical and electrochemical fields, and display enhanced mechanical, barrier and thermal properties.[18–20] However, free-standing anisotropic films based on LDH and guest molecules have not yet been achieved, due to the disordered stacking of the LDH host matrix and the random distribution of guest molecules in previously reported materials. From this viewpoint, designing 2D hybrid structures with layer-by-layer (LBL) characteristics constructed with magnetic LDH and fluorescent guests appears to be a feasible way in which to realize free-standing films with magnetic and fluorescence anisotropy simultaneously. The combination of a 2D inorganic matrix and fluorescent molecules for the fabrication of multifunctional films may result in the following advantages: first, the ordered magnetic LDH matrix would impart a high level of dispersion and orientation to the fluorescent molecule, which may endow the films with magnetic and luminescent anisotropy; second, the highly arrayed 2D-organized structure would inhibit the

State Key Laboratory of Chemical Resource Engineering, Beijing University of Chemical Technology, Beijing, 100029, China. E-mail: hanjb@mail.buct.edu.cn; Fax: +86-10-64425385; Tel: +86-10-64412131

† Electronic supplementary information (ESI) available: UV-vis spectra of the $(LDH/PVA)_n$ films (Fig. S1); fluorescence spectra of the $(LDH/PVA)_n$ films (Fig. S2); fluorescence spectra of the pristine BTBS solution and LDH/PVA/BTBS film (Fig. S3); UV-vis transmittance spectrum of the $(LDH/PVA/LDH/BTBS)_{300}$ film (Fig. S4); compositions of the $(LDH/PVA/LDH/BTBS)_{300}$ films (Table S1); room temperature (300 K) hysteresis loops for LDH (Fig. S5) and $(LDH/PVA/LDH/BTBS)_{300}$ films (Fig. S6); magnetic anisotropy for $(LDH/PVA/LDH/BTBS)_{300}$ films (Fig. S7); magnetic anisotropy for disordered LDH tablet (Fig. S8); magnetic anisotropy for oriented LDH film (Fig. S9); stress–strain curves (Fig. S10). See DOI: 10.1039/c3ta01674a

alignment of the spins of the LDH nanoplatelets in random directions and depress the aggregation of the fluorescent molecules, which is expected to enhance the magnetic and fluorescence properties.

Herein, flexible and robust LDH/PVA/LDH/BTBS free-standing films are fabricated by LBL assembly and subsequently the lift-off method (Scheme 1), and display both magnetic and luminescent anisotropy. Owing to the highly oriented 2D-organized structure, the free-standing films exhibit largely enhanced magnetic behavior and photoluminescence properties, compared with a disordered LDH/PVA/BTBS sample prepared by a solvent evaporation method. It is expected that this novel material with magnetic and luminescent anisotropy may have potential applications ranging from sensors to microfluidics and magneto-optical devices.

2 Experimental

2.1 Materials

The blue luminescent molecule, 2,2′-(1,2-ethenediyl)bis[5-[[4-(diethylamino)-6-[(2,5-disulfophenyl)amino]-1,3,5-triazin-2-yl]-amino]benzene sulfonic acid]hexasodium salt (abbreviated as BTBS, Scheme 1A) was purchased from Sigma-Aldrich. The chemicals HCl, NaOH, $Ni(NO_3)_2\cdot 6H_2O$, $Fe(NO_3)_3\cdot 9H_2O$, PVA, H_2SO_4, hydrofluoric acid and methanol used were of analytical grade and used without further purification. Deionized water was used in all the experimental processes.

2.2 Synthesis of LDH colloidal suspensions

A colloidal LDH suspension was prepared according to the separate nucleation and aging steps (SNAS) method reported by our group.[21,22] Typically, 100 ml of solution A ($Ni(NO_3)_2\cdot 6H_2O$: 0.2 M and $Fe(NO_3)_3\cdot 9H_2O$: 0.1 M) and 400 ml of solution B (NaOH: 0.15 M) were simultaneously added to a colloid mill with a rotor speed of 3000 rpm and mixed for 1 min. The resulting LDH slurry was obtained *via* centrifugation and washed with water and then dispersed in 400 ml of deionized water. The aqueous suspension was transferred into a stainless steel autoclave with a Teflon lining. After hydrothermal treatment at 110 °C for 24 h, a stable homogeneous NiFe–LDH suspension with a narrow size distribution was obtained. The concentrations of LDH nanoplatelets used for the fabrication of the film materials were 0.10%, 0.30% and 0.45% (wt%).

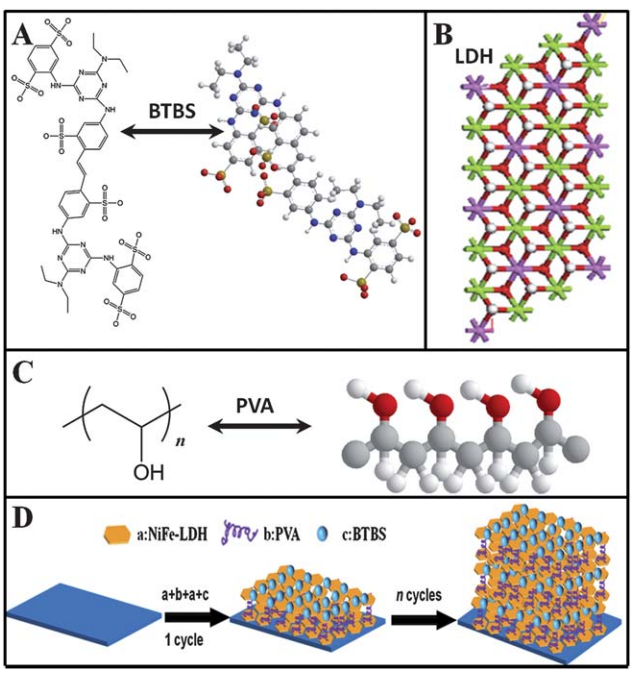

Scheme 1 Chemical structures of (A) BTBS, (B) LDH and (C) PVA. (D) Schematic representation of the LBL assembly of $(LDH/PVA/LDH/BTBS)_n$ films.

2.3 Fabrication of LDH/PVA/LDH/BTBS multilayer films

Multilayer films of $(LDH/PVA/LDH/BTBS)_n$ were fabricated by applying the layer-by-layer (LBL) assembly procedure. Prior to assembly, quartz glass slides were pretreated in a bath of methanol/HCl (1/1, v/v) and then concentrated H_2SO_4 for 30 min each to make the surface of the substrate hydrophilic and negatively charged. The deposition procedure was performed with a robotic manipulator (DR-3, R&K Technologies, Germany) programmed to carry out all the operations automatically for $n = 1$–300. The overall LBL process consisted of a cyclic repetition of the following steps: (a) dipping the pretreated substrates into the colloidal LDH suspension containing NiFe–LDH nanoplatelets for 10 min, followed by rinsing with deionized water thoroughly; (b) immersing the substrates in an aqueous solution of PVA ($M_w \approx 77\,000$, 1 wt%) for 10 min and washing with deionized water; (c) dipping the substrates into the colloidal LDH suspension containing NiFe–LDH nanoplatelets for 10 min, followed by rinsing with deionized water thoroughly; (d) immersing the substrates in an aqueous solution of BTBS (0.025 wt%) for 10 min and washing with deionized water. This series of operations was repeated n times to obtain $(LDH/PVA/LDH/BTBS)_n$ multilayer films. The resulting films were finally rinsed with deionized water and dried at ambient temperature. The free-standing films were released from the substrates by immersing them in 0.20 wt% aqueous hydrofluoric acid (pH adjusted to 5.5 with NaOH solution) for 30 min. The obtained films were picked up with a 60 mesh sieve and were finally dried under vacuum at room temperature. The following LDH based films were prepared as comparison samples:(1) $(LDH/PVA)_n$ film fabricated by an LBL method similar to that mentioned above, (2) LDH/PVA/BTBS film (LDH: 5.30 wt%; PVA: 92.75 wt%; BTBS: 1.95 wt%) obtained by a solvent evaporation method, (3) disordered LDH tablet prepared by a squash technique and (4) oriented LDH film fabricated by a spin-coating technique.

2.4 Characterization techniques

X-ray diffraction (XRD) patterns were recorded by a Rigaku XRD-6000 diffractometer, using Cu Kα radiation ($\lambda = 0.1542$ nm) at 40 kV, 30 mA. UV-vis absorption spectra were collected in the range 200–800 nm on a Shimadzu U-3000 spectrophotometer. Transmission electron microscopy (TEM) images were obtained using a JEOL JEM-2100 transmission electron microscope. The morphologies of the films were investigated using a scanning

electron microscope (SEM; Zeiss SUPRA 55) with an accelerating voltage of 20 kV and a NanoScope IIIa atomic force microscope (AFM) from Veeco Instruments. Fourier transform infrared (FT-IR) spectra were obtained using a Vector 22 (Bruker) spectrophotometer with a resolution of 2 cm^{-1}. The loading of LDH in the free-standing films was measured by inductively coupled plasma (ICP) emission spectroscopy (Shimadzu ICPS-7500). Fluorescence emission spectra were recorded in the range 365–650 nm, and both the excitation and emission slit were set to 3 nm. *In situ* fluorescence measurements of the UV-resistant capabilities of the films were performed on an RF-5301PC spectrofluorometer. The excitation light source was a 150 W xenon lamp (rated current: 7.5 A; maximal current: 8.0 A) with an excitation wavelength of 360 nm; both the excitation and emission slit were set to 3 nm. Steady-state polarized photoluminescence measurements of the films were recorded with an Edinburgh Instruments FLS 920 spectrofluorometer. The typical measurement mode was employed, with the excitation beam parallel and vertical to the film (glancing and normal incidence geometry, respectively). Fluorescence decay profiles were measured by exciting the films with a 360 nm laser in a LifeSpec-ps spectrometer, and the fluorescence lifetimes of the total decay were calculated with F900 Edinburgh instruments software. The magnetism of the films was measured on an LDJ 9600 vibration sample magnetometer. The mechanical properties of the free-standing hybrid films were measured under tensile mode in a universal mechanical testing machine (Instron, FastTrack 8800 Servohydraulic Systems) with a load speed of 0.5 mm min^{-1}. Free-standing specimens were obtained by cutting the film into 4 mm wide and 20 mm long strips. The mechanical properties (tensile strength and strain at rupture) recorded of the specimens were the average of five different strips of the same sample.

3 Result and discussion

3.1 Assembly of the $(LDH/PVA/LDH/BTBS)_n$ films

In this work, a colloidal suspension of magnetic NiFe–LDH was prepared according to the separate nucleation and aging steps method reported by our group.[21,22] Fig. 1A shows the XRD pattern of the NiFe–LDH sample, which can be indexed as a hexagonal structure with $2\theta = 10.2°$, 22.5°, 33.8°, 37.5°, 45.5°, 58.8°and 61.1° (corresponding lattice parameters: $d_{003} = 8.67$ Å, $d_{006} = 3.95$ Å, $d_{009} = 2.65$ Å, $d_{012} = 2.40$ Å, $d_{018} = 1.99$ Å, $d_{110} = 1.57$ Å and $d_{113} = 1.54$ Å). No other crystalline phase was detected, indicating the high purity of the product. Moreover, the FT-IR spectrum (Fig. 1B) provides evidence for the presence of nitrate in the LDH interlayer (band at 1383 cm^{-1}); no absorption at 1356 cm^{-1} was observed, indicating the absence of carbonate. The TEM image reveals the hexagonal LDH nanoplatelets (Fig. 1C), and the corresponding selected-area electron diffraction (SAED) pattern (inset) exhibits hexagonally arranged bright spots, confirming the single-crystal nature of the LDH phase. Clear Tyndall light scattering was observed (Fig. 1D), and the well-dispersed suspension was stable without any precipitation when stored in an N_2 atmosphere for more than one month.

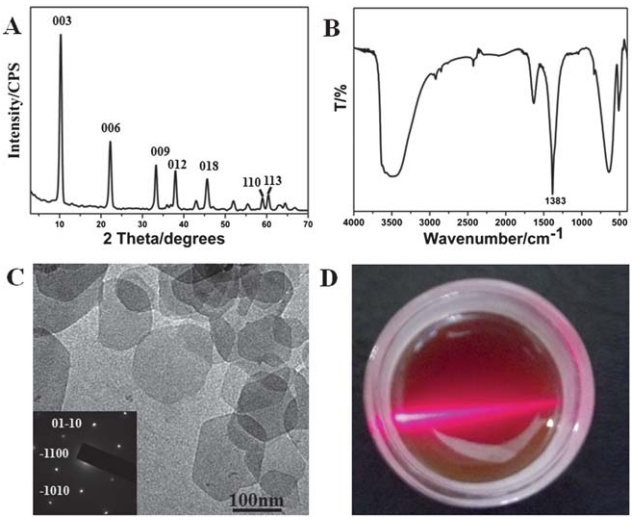

Fig. 1 Characterization of the NiFe–LDH: (A) powder XRD pattern; (B) FT-IR spectrum; (C) TEM image (inset: the corresponding SAED pattern) and (D) digital photograph of its colloidal suspension.

The NiFe–LDH nanoplatelets were then used as building blocks to fabricate $(LDH/PVA/LDH/BTBS)_n$ films and $(LDH/PVA)_n$ films (for comparison) by the LBL assembly method. The assembly process was monitored by UV-vis absorption and fluorescence emission spectroscopy. The $(LDH/PVA/LDH/BTBS)_n$ films exhibit a strong absorption band at 344 nm, which is attributed to the characteristic absorption band of BTBS (Fig. 2A), while the $(LDH/PVA)_n$ films display no obvious

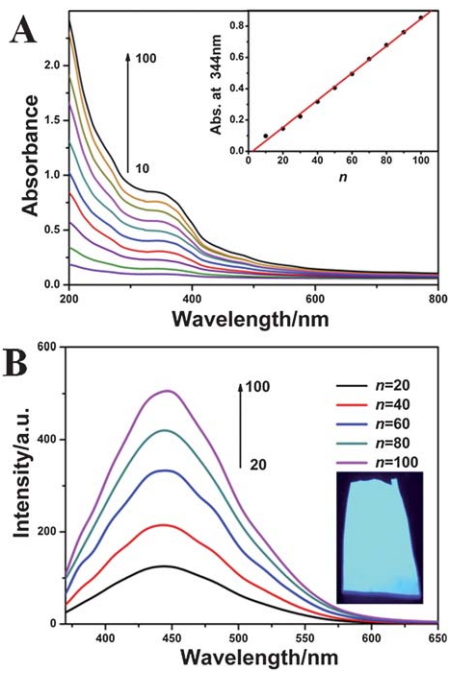

Fig. 2 (A) UV-vis spectra of the $(LDH/PVA/LDH/BTBS)_n$ ($n = 10$–100) films (inset: the linear relationship between the absorbance at 344 nm and n); (B) fluorescence spectra of the $(LDH/PVA/LDH/BTBS)_n$ ($n = 20$–100) films (inset: photograph of the film irradiated by 365 nm UV-light).

absorption band in the range 200–800 nm (Fig. S1, ESI†). The inset in Fig. 2A shows that the intensity of the characteristic absorption band of BTBS at 344 nm increases linearly with the tetra-layer number n. Furthermore, the fluorescence emission intensity at 445 nm attributed to BTBS also displays a consistent enhancement as n is increased (Fig. 2B), in contrast to the (LDH/PVA)$_n$ films which do not display a fluorescence emission band in the range 370–650 nm (Fig. S2, ESI†), demonstrating a stepwise and regular film growth procedure. Meanwhile, the thin film under UV light irradiation (Fig. 2B) also reveals well-defined blue luminescence. In addition, compared with the fluorescence spectrum of pristine BTBS solution, the fluorescence spectrum of the LDH/PVA/BTBS film prepared by solvent evaporation technology reveals a red shift of 11 nm (Fig. S3, ESI†), indicating the formation of BTBS aggregates. However, no obvious red or blue shift was observed for the (LDH/PVA/LDH/BTBS)$_n$ films, illustrating the absence of BTBS aggregation throughout the LBL assembly process.

3.2 Structural and morphological study of the (LDH/PVA/LDH/BTBS)$_n$ films

The XRD patterns (Fig. 3A) for the obtained (LDH/PVA/LDH/BTBS)$_n$ (n = 100, 200 and 300) films display a peak at 2θ = 10.2°, which is attributed to the (003) reflection of the LDH structure (the peak at 2θ = 15–30° is assigned to the amorphous reflection of the quartz substrate).[23,24] The absence of any nonbasal reflections (h, $l \neq 0$) compared with the LDH powdered sample (Fig. 1A) indicates a preferred orientation of LDH platelets with the ab plane parallel to the substrate. After being released from the substrate, the (LDH/PVA/LDH/BTBS)$_{300}$ free-standing film exhibits good uniformity, flexibility (Fig. 3B) and high transparency (50 to 70% across the visible light region, Fig. S4, ESI†). The top view of the SEM image displays a smooth and continuous surface (Fig. 3C), and the cross-sectional SEM image (Fig. 3C, inset) reveals a well-defined layered structure. The AFM image shown in Fig. 3D with a value of the root-mean-square roughness of 12.4 nm indicates a relatively smooth surface.

3.3 Magnetic properties of the (LDH/PVA/LDH/BTBS)$_n$ films

The low-temperature (10 K) magnetic behaviors of the (LDH/PVA/LDH/BTBS)$_{300}$ films with various weight fractions (see details in the ESI, Table S1†) of LDH (W_L) were investigated (Fig. 4). The saturation magnetization (M_s) for the LDH/PVA/BTBS film (W_L = 5.30%) prepared by solvent evaporation technology was measured as 0.49 emu g^{-1}. In contrast, the (LDH/PVA/LDH/BTBS)$_{300}$ film with the same W_L value (W_L = 5.30%) displays a higher M_s (0.89 emu g^{-1}), which is probably related to the ordered magnetic interaction and suitable distance between the adjacent spins of the LDH nanoplatelets in such a highly oriented 2D-organized structure. As the W_L is increased from 5.30% to 10.14%, the M_s of the (LDH/PVA/LDH/BTBS)$_{300}$ film is enhanced from 0.89 to 2.18 emu g^{-1}. Although the magnetic properties of the (LDH/PVA/LDH/BTBS)$_{300}$ film were enhanced, its M_s was lower than the typical value of high performance magneto-optical films (>30 emu g^{-1}).[1a,2c,5c] This is attributed to the limitation of the intrinsic weak magnetic properties of the NiFe–LDH (M_s = 8.23 emu g^{-1}, Fig. S5, ESI†). The hysteresis loops of the (LDH/PVA/LDH/BTBS)$_{300}$ films at room temperature (300 K) (Fig. S6, ESI†) display the typical "S" shape with a small detectable remnant magnetization (M_r) and coercive force (H_c), indicating that the free-standing films are soft magnetic materials. Moreover, the films have sufficient magnetization to be held up by a magnet (inset of Fig. 4).

3.4 Magnetic and luminescent anisotropy of the (LDH/PVA/LDH/BTBS)$_n$ films

The magnetic and luminescent anisotropy of the (LDH/PVA/LDH/BTBS)$_{300}$ film was further investigated. The hysteresis

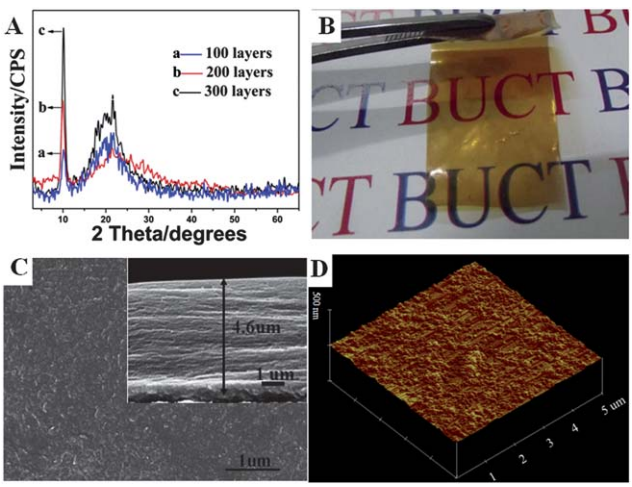

Fig. 3 (A) XRD patterns of the (LDH/PVA/LDH/BTBS)$_n$ (n = 100, 200, 300) films; (B) photograph of the (LDH/PVA/LDH/BTBS)$_{300}$ free-standing film released from the substrate; (C) top-view SEM image (inset: side-view SEM image) and (D) AFM image for the (LDH/PVA/LDH/BTBS)$_{300}$ free-standing film.

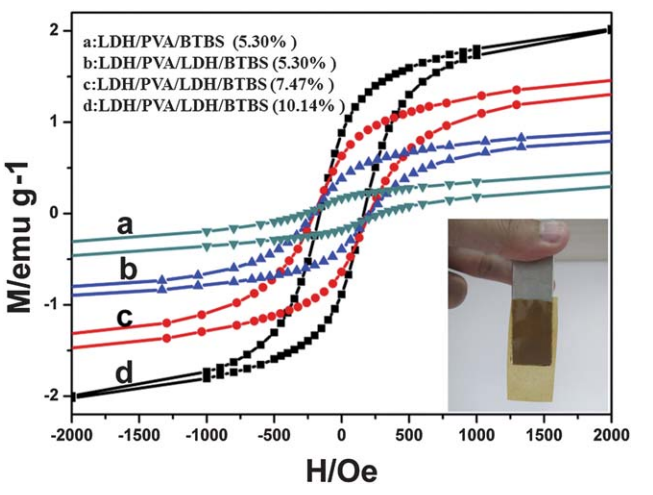

Fig. 4 Low temperature (10 K) hysteresis loops measured in the perpendicular direction for (a) LDH/PVA/BTBS films with LDH weight fractions (W_L) of 5.30% and (LDH/PVA/LDH/BTBS)$_{300}$ films with various W_L (b: 5.30%; c: 7.47% and d: 10.14%) (inset: photograph of the (LDH/PVA/LDH/BTBS)$_{300}$ film held up by a magnet).

loops of the film measured at 10 K (Fig. 5A) and 300 K (Fig. S7, ESI†) show that H_c and M_r are much higher in the perpendicular direction than in the parallel direction, which demonstrates the magnetic anisotropy of the $(LDH/PVA/LDH/BTBS)_{300}$ film. Similar results have also been reported previously based on $(CoFe–LDH/manganese\ porphyrin)_n$ multilayer films.[24c] However, no magnetic anisotropy was found for the LDH/PVA/BTBS film (Fig. 5B). Meanwhile, the magnetic anisotropy for the disordered LDH tablet (obtained by a squash technique, Fig. S8, ESI†) and the oriented LDH film (fabricated by a spin-coating method, Fig. S9, ESI†) was measured to investigate the intrinsic magnetic behavior of the LDH nanoplatelets. The results revealed that only the oriented LDH films displayed magnetic anisotropy, and the disordered LDH tablets did not, demonstrating that a high level of orientation of the LDH nanoplatelets renders the magnetic anisotropy of $(LDH/PVA/LDH/BTBS)_{300}$ and spin-coated LDH films.

Moreover, the oriented LDH matrix and $(LDH/PVA/LDH/BTBS)_n$ films displayed similar magnetic anisotropy behavior, illustrating that the magnetic anisotropy for the $(LDH/PVA/LDH/BTBS)_n$ films depended on the intrinsic anisotropy of the oriented LDH matrix. Therefore, these observations reveal that the oriented stacking of magnetic LDH nanoplatelets is beneficial to the anisotropic properties of the $(LDH/PVA/LDH/BTBS)_{300}$ film. Moreover, anisotropic photoluminescence spectroscopy demonstrates that the free-standing film exhibited strong polarized fluorescence with an anisotropy value of 0.20 (Fig. 6A). The uniform r value in the range 420–550 nm indicates that the weight fraction of the LDH imposes no obvious influence on the macroscopic polarized luminescence characteristics of the $(LDH/PVA/LDH/BTBS)_{300}$ film throughout the whole fabrication process (Fig. 6B, curves b, c and d). In addition, no polarization was found for the disordered LDH/PVA/BTBS film (Fig. 6B, curve a). The polarized fluorescence of the $(LDH/PVA/LDH/BTBS)_{300}$ films is attributed to an ordered distribution of the BTBS cations between the LDH layers, resulting from the highly oriented 2D-organized structure. Therefore, the $(LDH/PVA/LDH/BTBS)_{300}$ films exhibit enhanced magnetic and optical performances with anisotropy, and can serve as promising candidates for magneto-optical materials.

3.5 Stability of the $(LDH/PVA/LDH/BTBS)_n$ films

UV-resistance capability is a key factor for the practical application of luminescent films. Upon UV irradiation,

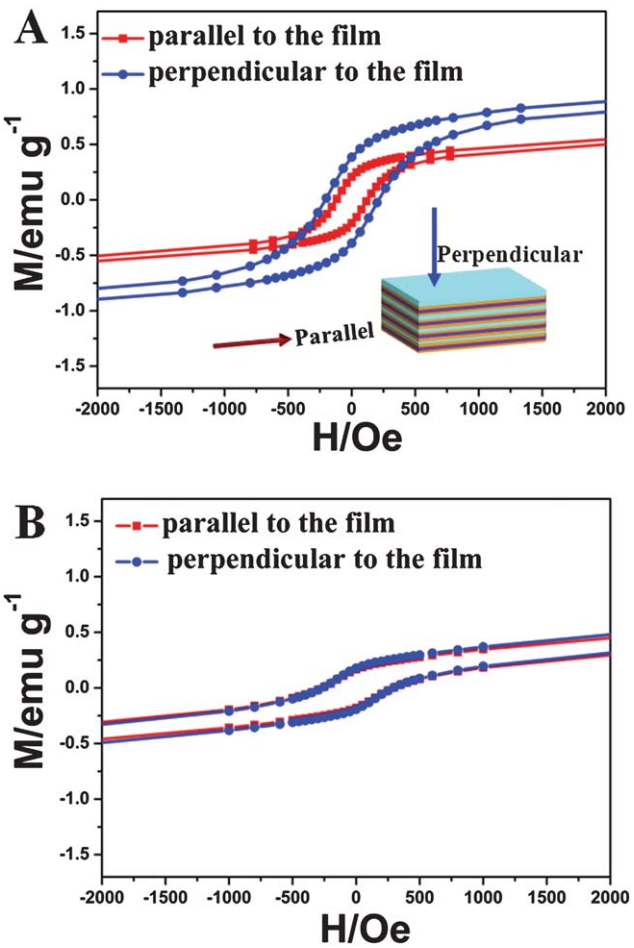

Fig. 5 Low temperature (10 K) hysteresis loops for both orientations for (A) the $(LDH/PVA/LDH/BTBS)_{300}$ film and (B) the LDH/PVA/BTBS film prepared by the solvent evaporation method.

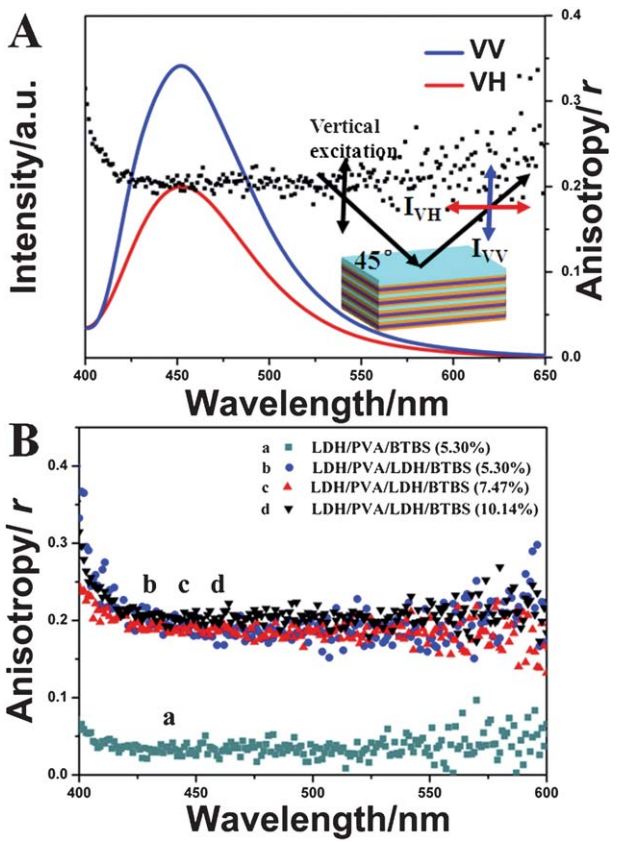

Fig. 6 (A) Polarized fluorescence profiles with glancing incidence geometry in the VV, VH modes and (B) anisotropic value (r) for (a) the disordered LDH/PVA/BTBS film with $W_L = 5.30\%$ and the ordered $(LDH/PVA/LDH/BTBS)_{300}$ films with various W_L values (b: 5.30%; c: 7.47% and d: 10.14%).

the normalized fluorescence intensity of the (LDH/PVA/LDH/BTBS)$_{300}$ film is systematically larger than that of the LDH/PVA/BTBS film prepared by the solvent evaporation method (Fig. 7A). The results demonstrate that the UV-resistance capability of BTBS is enhanced significantly, since the inorganic LDH host layers can reflect and absorb UV light effectively.[25] Furthermore, the fluorescence lifetime of the (LDH/PVA/LDH/BTBS)$_{300}$ film is prolonged compared to that of the LDH/PVA/BTBS film (Fig. 7B). This remarkable increase is related to the isolation effect imposed by the rigid LDH layers, which prevents the formation of chromophore aggregates and thus enhances the luminescent properties. In addition, typical stress–strain curves (Fig. S10, see details in the ESI†) demonstrate that the (LDH/PVA/LDH/BTBS)$_{300}$ films exhibit high strength and excellent ductility simultaneously, which is ascribed to the arrayed incorporation of inorganic nanoplatelets into the PVA organic matrix, which guarantees their practical applications.

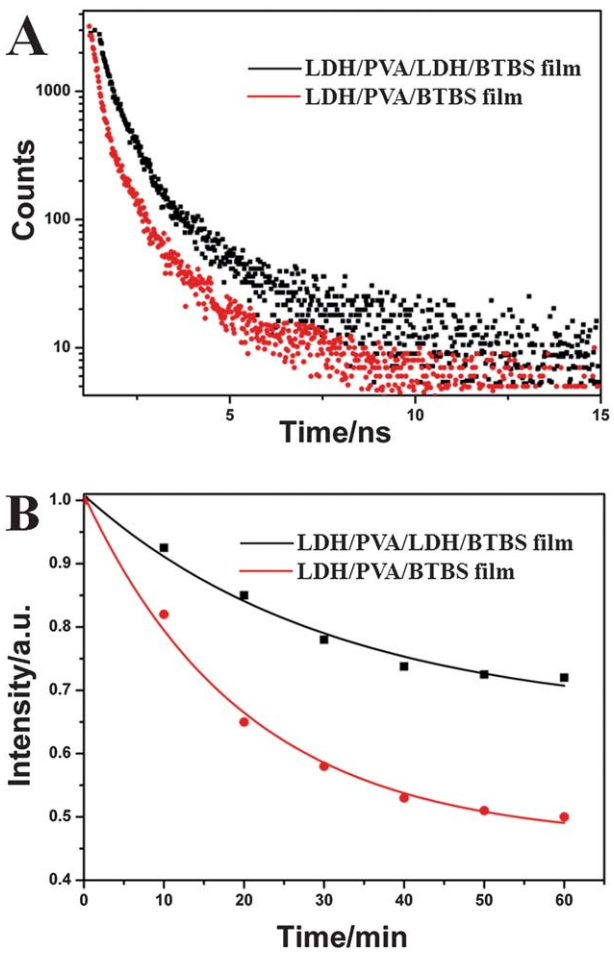

Fig. 7 (A) The decay of normalized maximal fluorescence intensity with irradiation time (360 nm UV light) for probing the UV-light-resistance capability and (B) comparison of the fluorescence decay profiles for the (a) the disordered LDH/PVA/BTBS film and (b) the ordered (LDH/PVA/LDH/BTBS)$_{300}$ film with the same composition (LDH: 5.30 wt%; PVA: 92.75 wt%; BTBS: 1.95 wt%).

4 Conclusions

In summary, transparent free-standing films with magnetic and luminescent anisotropy were fabricated by the LBL assembly method. Structural and morphological studies show that the films were continuous and uniform with long range stacking order. In contrast to the LDH/PVA/BTBS film prepared by the solvent evaporation method, the (LDH/PVA/LDH/BTBS)$_n$ films exhibited enhanced magnetic and optical properties, including higher saturation magnetization, longer luminescence lifetime and stronger polarized photoemission. More significantly, the 2D-organized structure induced an ordered stacking of LDH nanoplatelets and uniform dispersion of the BTBS anions, which resulted in enhanced magnetic and luminescent anisotropy. Therefore, this work provides a facile method for the fabrication of anisotropic 2D-organized materials based on the LDH/PVA/LDH/BTBS system, which can be potentially used in magneto-optical sensors, magnetic data storage and magnetic devices.

Acknowledgements

This work was supported by the National Natural Science Foundation of China, the 973 Program (grant no. 2011CBA00504), the 111 Project (grant no. B07004), the Collaboration Project from the Beijing Education Committee and the Fundamental Research Funds for the Central Universities (grant no. ZY1215).

Notes and references

1 (*a*) K. Hayashi, R. Fujikawa, W. Sakamoto, M. Inoue and T. Yogo, *J. Phys. Chem. C*, 2008, **112**, 14255; (*b*) J. Gao, B. Zhang, Y. Gao, Y. Pan, X. Zhang and B. Xu, *J. Am. Chem. Soc.*, 2007, **129**, 11928; (*c*) H. Gu, R. Zheng, X. Zhang and B. Xu, *J. Am. Chem. Soc.*, 2004, **126**, 5664.

2 (*a*) K. Guo, M. Y. Berezin, J. Zheng, W. Akers, F. Lin, B. Teng, O. Vasalatiy, A. Gandjbakhche, G. L. Griffiths and S. Achilefu, *Chem. Commun.*, 2010, **46**, 3705; (*b*) K. Ishii and K. Ozawa, *J. Phys. Chem. C*, 2009, **113**, 18897; (*c*) D. Fragouli, R. Buonsanti, G. Bertoni, C. Sangregorio, C. Innocenti, A. Falqui, D. Gatteschi, P. D. Cozzoli, A. Athanassiou and R. Cingolani, *ACS Nano*, 2010, **4**, 1873.

3 (*a*) D. Weller, *IEEE Trans. Magn.*, 2000, **36**, 10; (*b*) J. Gong, S. Li, D. Zhang, X. Zhang, C. Liu and Z. Tong, *Chem. Commun.*, 2010, **46**, 3514; (*c*) M. Rubio-Roy, O. Vlasin, O. Pascu, J. M. Caicedo, M. Schmidt, A. R. Goñi, N. G. Tognalli, A. Fainstein, A. Roig and G. Herranz, *Langmuir*, 2012, **28**, 9010; (*d*) X. Yu, Y. Shan, G. Li and K. Chen, *J. Mater. Chem.*, 2011, **21**, 8104.

4 B. P. Pichon, M. Pauly, P. Marie, C. Leuvrey and S. Begin-Colin, *Langmuir*, 2011, **27**, 6235.

5 (*a*) L. M. Toma, R. Lescouëzec, J. Pasán, C. Ruiz-Párez, J. Vaissermann, J. Cano, R. Carrasco, W. Wernsdorfer, F. Lloret and M. Julve, *J. Am. Chem. Soc.*, 2006, **128**, 4842; (*b*) D. M. Pajerowski, J. E. Gardner, D. R. Talhamand and M. W. Meisel, *New J. Chem.*, 2011, **35**, 1320; (*c*)

E. M. Moreno, M. Zayat, M. P. Morales, C. J. Serna, A. Roig and D. Levy, *Langmuir*, 2002, **18**, 4972.

6 (*a*) K. Bernot, J. Luzon, R. Sessoli, A. Vindigni, J. Thion, S. Richeter, D. Leclercq, J. Larionova and A. van der Lee, *J. Am. Chem. Soc.*, 2008, **130**, 1619; (*b*) W. C. Molenkamp, M. Watanabe, H. Miyata and S. H. Tolbert, *J. Am. Chem. Soc.*, 2004, **126**, 4476; (*c*) Y. Bai, J. Tao, W. Wernsdorfer, O. Sato, R. Huang and L. Zheng, *J. Am. Chem. Soc.*, 2006, **128**, 16428; (*d*) H. Xu, B. Wang, F. Pan, Z. Wang and S. Gao, *Angew. Chem., Int. Ed.*, 2007, **46**, 7388.

7 (*a*) M. Nakano and H. Oshio, *Chem. Soc. Rev.*, 2011, **40**, 3239; (*b*) L. Lecren, O. Roubeau, C. Coulon, Y. Li, X. F. L. Goff, W. Wernsdorfer, H. Miyasaka and R. Clérac, *J. Am. Chem. Soc.*, 2005, **127**, 17353; (*c*) Z. Liu, R. Ma, M. Osada, N. Iyi, Y. Ebina, K. Takada and T. Sasaki, *J. Am. Chem. Soc.*, 2006, **128**, 4872.

8 (*a*) E. Coronado, J. R. Galan-Mascaros and C. Marti-Gastaldo, *Inorg. Chem.*, 2007, **46**, 8108; (*b*) P. Mahata, S. Natarajan, P. Panissod and M. Drillon, *J. Am. Chem. Soc.*, 2009, **131**, 10140; (*c*) D. Pinkowicz, R. Pełka, O. Drath, W. Nitek, M. Bałanda, A. M. Majcher, G. Poneti and B. Sieklucka, *Inorg. Chem.*, 2010, **49**, 7565.

9 M. S. Mauter, M. Elimelech and C. O. Osuji, *ACS Nano*, 2011, **4**, 6651.

10 W. C. Molenkamp, M. Watanabe, H. Miyata and S. H. Tolbert, *J. Am. Chem. Soc.*, 2004, **126**, 4476.

11 (*a*) C. A. Breen, T. Deng, T. Breiner, E. L. Thomas and T. M. Swager, *J. Am. Chem. Soc.*, 2003, **125**, 9942; (*b*) J. Wu, A. F. Gross and S. H. Tolbert, *J. Phys. Chem. B*, 1999, **103**, 2374.

12 P. Podsiadlo, Z. Liu, D. Paterson, P. B. Messersmith and N. A. Kotov, *Adv. Mater.*, 2007, **19**, 949.

13 (*a*) B. L. Smith, T. E. Schäffer, M. J. Viani, B. Thompson, N. A. Frederick, J. Kindt, A. Belcher, G. D. Stucky, D. E. Morse and P. K. Hansma, *Nature*, 1999, **399**, 761; (*b*) S. Dutta and S. K. Pati, *J. Mater. Chem.*, 2010, **20**, 8207.

14 H. Yao, Y. Guan, L. Mao, Y. Wang, X. Wang, D. Tao and S. Yu, *J. Mater. Chem.*, 2012, **22**, 13005.

15 (*a*) Q. Wang and D. O'Hare, *Chem. Rev.*, 2012, **112**, 4124; (*b*) G. R. Williams and D. O'Hare, *J. Mater. Chem.*, 2006, **16**, 3065; (*c*) D. Yan, J. Lu, J. Ma, S. Qin, M. Wei, D. G. Evans and X. Duan, *Angew. Chem., Int. Ed.*, 2011, **50**, 7037; (*d*) A. Illaik, C. Taviot-Guého, J. Lavis, S. Commereuc, V. Verney and F. Leroux, *Chem. Mater.*, 2008, **20**, 4854; (*e*) J. Y. Uan, J. K. Lin and Y. S. Yung, *J. Mater. Chem.*, 2010, **20**, 761; (*f*) A. M. Fogg, V. M. Green, H. G. Harvey and D. O'Hare, *Adv. Mater.*, 1999, **11**, 1466; (*g*) X. Hou and R. J. Kirkpatrick, *Inorg. Chem.*, 2001, **40**, 6397; (*h*) W. Shi, Y. Lin, S. He, Y. Zhao, C. Li, M. Wei, D. G. Evans and X. Duan, *J. Mater. Chem.*, 2011, **21**, 11116; (*i*) B. Monteiro, S. Gago, F. A. A. Paz, R. Bilsborrow, I. S. Gonçalves and M. Pillinger, *Inorg. Chem.*, 2008, **47**, 8674; (*j*) F. Leroux and C. Taviot-Guého, *J. Mater. Chem.*, 2005, **15**, 3628; (*k*) W. Shi, S. He, M. Wei, D. G. Evans and X. Duan, *Adv. Funct. Mater.*, 2010, **20**, 3856.

16 (*a*) M. C. Richardson and P. S. Braterman, *J. Phys. Chem. C*, 2007, **111**, 4209; (*b*) J. W. Bocair and P. S. Braterman, *Chem. Mater.*, 1999, **11**, 298; (*c*) D. Yan, J. Lu, M. Wei, D. G. Evans and X. Duan, *J. Mater. Chem.*, 2011, **21**, 13128; (*d*) S. Gago, T. Costa, J. S. de Melo, I. S. Gonçalves and M. Pillinger, *J. Mater. Chem.*, 2008, **18**, 894; (*e*) S. Gago, M. Pillinger, R. A. S. Ferreira, L. D. Carlos, T. M. Santos and I. S. Gonçalves, *Chem. Mater.*, 2005, **17**, 5803; (*f*) X. Hou and R. J. Kirkpatrick, *Chem. Mater.*, 2002, **14**, 1195; (*g*) X. Zhao, F. Zhang, S. Xu, D. G. Evans and X. Duan, *Chem. Mater.*, 2010, **22**, 3933; (*h*) J. L. Gunjakar, T. W. Kim, H. N. Kim, I. Y. Kim and S. J. Hwang, *J. Am. Chem. Soc.*, 2011, **133**, 14998; (*i*) J. A. Kim, S. J. Hwang and J. H. Choy, *J. Nanosci. Nanotechnol.*, 2008, **8**, 5172.

17 (*a*) D. Yan, J. Lu, L. Chen, S. Qin, J. Ma, M. Wei, D. G. Evans and X. Duan, *Chem. Commun.*, 2010, **46**, 5912; (*b*) A. Illaik, C. Taviot-Guého, J. Lavis, S. Commereuc, V. Verney and F. Leroux, *Chem. Mater.*, 2008, **20**, 4854; (*c*) A. W. Myong, M. S. Song, T. W. Kim, I. Y. Kim, J. Y. Ju, Y. S. Lee, S. J. Kim, J. H. Choy and S. J. Hwang, *J. Mater. Chem.*, 2011, **21**, 4286.

18 (*a*) A. W. Myong, M. S. Song, T. W. Kim, I. Y. Kim, J. Y. Ju, Y. S. Lee, S. J. Kim, J. H. Choy and S. J. Hwang, *J. Mater. Chem.*, 2011, **21**, 4286; (*b*) Q. Wang, H. Tay, D. Ng, L. Chen, Y. Liu, J. Chang, Z. Zhong, J. Luo and A. Borgna, *ChemSusChem.*, 2010, **3**, 965.

19 J. Y. Uan, J. K. Lin and Y. S. Yung, *J. Mater. Chem.*, 2010, **20**, 761.

20 S. Gago, T. Costa, J. S. de Melo, I. S. Gonçalves and M. Pillinger, *J. Mater. Chem.*, 2008, **18**, 894.

21 J. Han, Y. Dou, M. Wei, D. G. Evans and X. Duan, *Angew. Chem., Int. Ed.*, 2010, **49**, 2171.

22 Y. Zhao, F. Li, R. Zhang, D. G. Evans and X. Duan, *Chem. Mater.*, 2002, **14**, 4286.

23 J. Gursky, S. Blough, C. Luna, C. Gomez, A. Luevano and E. Gardner, *J. Am. Chem. Soc.*, 2006, **128**, 8376.

24 (*a*) M. Adachi-Pagano, C. Forano and J. P. Besse, *Chem. Commun.*, 2000, **36**, 91; (*b*) E. Gardner, K. Huntoon and T. Pinnavaia, *Adv. Mater.*, 2001, **13**, 1263; (*c*) M. Shao, M. Wei, D. G. Evans and X. Duan, *Chem. Commun.*, 2011, **47**, 3171.

25 D. Yan, J. Lu, M. Wei, S. Li, D. G. Evans and X. Duan, *Phys. Chem. Chem. Phys.*, 2012, **14**, 85913.

